NUCLEAR THEORY, Vol. 40 (2023)
eds. M. Gaidarov, N. Minkov, Heron Press, Sofia

Rotating Deformed Halo Nuclei

X.-X. Sun[1,2], **S.-G. Zhou**[1,2,3,4]

[1]CAS Key Laboratory of Theoretical Physics, Institute of Theoretical Physics, Chinese Academy of Sciences, Beijing 100190, China
[2]School of Nuclear Science and Technology, University of Chinese Academy of Sciences, Beijing 100049, China
[3]School of Physical Sciences, University of Chinese Academy of Sciences, Beijing 100049, China
[4]Peng Huanwu Collaborative Center for Research and Education, Beihang University, Beijing 100191, China

Abstract. Deformed halo is one of the most notable exotic nuclear structures. The deformed relativistic Hartree-Bogoliubov theory in continuum (DRHBc) has been developed and achieved self-consistent descriptions of deformed halo nuclei by including deformation and continuum effects. The DRHBc theory has been used to study the ground states of deformed halo nuclei and predict an interesting phenomenon, the shape decoupling between the core and the halo. In this contribution, the implementation of the angular momentum projection technique based on the DRHBc theory and its application in rotationally excited deformed halo nuclei are briefly presented. It has been shown that the halo structures and shape decoupling effects also exist in the low-lying rotational states of deformed halo nuclei.

1 Introduction

With the development of rare-ion-beam facilities worldwide, many exotic nuclear phenomena have been observed in nuclei far from the β-stability line, such as cluster structures, neutron halos and proton halos, neutron skins, and the appearance of new magic numbers [1,2,4–7]. The study of exotic nuclear phenomena including nuclear halos is currently at the forefront of nuclear physics. The first observed halo nucleus is ^{11}Li in 1985 [8]. In recent years, the neutron halos in ^{31}Ne [9], ^{37}Mg [10], ^{17,19}B [11, 12] and ^{29}F [13] have been confirmed experimentally. The nuclear halos are characterized by weak binding and large spatial extension due to the occupation of low-l (s- or p-wave) orbitals by valence nucleon(s) [1, 4, 14]. Due to the long-range quantum correlations, a weakly bound nucleus with halo can be deformed and ^{31}Ne [9] and ^{37}Mg [10] are representative examples. The shapes of a nucleus can be directly connected to collective motion featured by typical excitation spectra. Thus it is interesting and meaningful to study the excitation of deformed halo nuclei.

In 2010, self-consistent descriptions for the ground states of deformed halo nuclei have been achieved by using the deformed relativistic Hartree-Bogoliubov

theory in continuum (DRHBc) [15]. With this theory, ^{42,44}Mg are predicted as deformed halo nuclei with shape decoupling effects: The core has a prolate shape while the halo is slightly oblate [15,16]. Afterwards, many deformed halo nuclei including ^{15,22}C [17, 18] and ^{17,19}B [11, 19], have been studied by using the DRHBc theory and the theoretical results are reasonably consistent with available measurements. The DRHBc theory is also used to construct nuclear mass table [20–22] and many interesting nuclear structures have been studied based on the global DRHBc calculations [23–32]. Additionally, the predictions of deformed halos have also been made by using non-relativistic density functional theories [33,34].

Within the nuclear density functional theory, the self-consistent descriptions of low-lying excited states can be achieved by developing beyond-mean-field (BMF) approaches, such as the angular momentum projection (AMP) and generator coordinate method (GCM) [35, 36]. Such BMF calculations have been well established based on non-relativistic or relativistic mean-field models by expanding the wave function in analytical harmonic oscillator (HO) bases [37,38], which, however, do not provide a proper description of the asymptotic behavior of wave functions for weakly bound nuclei. It has been shown in Ref. [39] that the Woods-Saxon (WS) basis is suitable for weakly bound nuclei. The projected wave function can be expanded in terms of the Dirac WS basis [39] such that BMF calculations can be applied to deformed halo nuclei. Along this line, the AMP has been implemented to the DRHBc theory to study rotational excitations of deformed halo nuclei [40,41].

In this contribution, the implementation of AMP based on the DRHBc theory will be introduced and its application in deformed halo nuclei and the typical behavior of shape decoupling effects in rotational states will be presented.

2 Theoretical Framework

The starting point of relativistic mean-field theory is a Lagrangian density where nucleons are described as Dirac spinors which interact via exchange of effective mesons (σ, ω, and ρ) and the photon

$$\begin{aligned}\mathcal{L} &= \bar{\psi}(i\partial\!\!\!/ - M)\psi + \frac{1}{2}\partial_\mu\sigma\partial^\mu\sigma - U(\sigma) - g_\sigma\bar{\psi}\sigma\psi \\ &- \frac{1}{4}\Omega_{\mu\nu}\Omega^{\mu\nu} + \frac{1}{2}m_\omega^2\omega_\mu\omega^\mu - g_\omega\bar{\psi}\omega\!\!\!/\psi \\ &- \frac{1}{4}\vec{R}_{\mu\nu}\vec{R}^{\mu\nu} + \frac{1}{2}m_\rho^2\vec{\rho}_\mu\vec{\rho}^\mu - g_\rho\bar{\psi}\vec{\rho}\!\!\!/\cdot\vec{\tau}\psi \\ &- \frac{1}{4}F_{\mu\nu}F^{\mu\nu} - e\bar{\psi}\frac{1-\tau_3}{2}A\!\!\!/\psi, \end{aligned} \tag{1}$$

where M is the nucleon mass and m_σ, m_ω, m_ρ, g_σ, g_ω, and g_ρ are masses and coupling constants of the respective mesons. U is the nonlinear self-coupling for the scalar meson.

The detailed formulae for the DRHBc theory can be found in Refs. [15, 16]. Here we give briefly the main ones for convenience of discussions. The relativistic Hartree-Bogoliubov (RHB) equation for nucleons reads,

$$\begin{pmatrix} h_D - \lambda_\tau & \Delta \\ -\Delta^* & -h_D^* + \lambda_\tau \end{pmatrix} \begin{pmatrix} U_k \\ V_k \end{pmatrix} = E_k \begin{pmatrix} U_k \\ V_k \end{pmatrix}, \tag{2}$$

which is solved in a Dirac WS basis [39]. E_k is the quasi particle energy, λ_τ ($\tau = \mathrm{n}, \mathrm{p}$) is the chemical potential, and U_k and V_k are quasi particle wave functions. h_D is the Dirac Hamiltonian

$$h_\mathrm{D} = \boldsymbol{\alpha} \cdot \boldsymbol{p} + V(\boldsymbol{r}) + \beta[M + S(\boldsymbol{r})], \tag{3}$$

where $S(\boldsymbol{r})$ and $V(\boldsymbol{r})$ are scalar and vector potentials. The pairing potential reads

$$\Delta(\boldsymbol{r}_1, \boldsymbol{r}_2) = V^{pp}(\boldsymbol{r}_1, \boldsymbol{r}_2)\kappa(\boldsymbol{r}_1, \boldsymbol{r}_2), \tag{4}$$

where we use a density dependent zero-range force in the particle-particle channel,

$$V^{pp}(\boldsymbol{r}_1, \boldsymbol{r}_2) = \frac{1}{2}V_0(1 - P^\sigma)\delta(\boldsymbol{r}_1, \boldsymbol{r}_2)\left(1 - \frac{\rho(\boldsymbol{r}_1)}{\rho_\mathrm{sat}}\right), \tag{5}$$

and $\kappa(\boldsymbol{r}_1, \boldsymbol{r}_2)$ is the pairing tensor [42].

For axially deformed nuclei with spatial reflection symmetry, we expand densities and potentials in terms of Legendre polynomials,

$$f(\boldsymbol{r}) = \sum_\lambda f_\lambda(r)P_\lambda(\cos\theta), \quad \lambda = 0, 2, 4, \cdots, \tag{6}$$

with

$$f_\lambda(r) = \frac{2\lambda + 1}{4\pi}\int d\Omega f(\boldsymbol{r})P_\lambda(\cos\theta). \tag{7}$$

A low-lying rotational state $|JM\rangle$ with the angular momentum J and its projection M along the z axis in laboratory frame can be constructed by performing the AMP on the intrinsic wave function $|\Phi(\beta_2)\rangle$ obtained from DRHBc calculations with a certain quadrupole deformation parameter β_2

$$|\Psi^{JM}\rangle = f^J\hat{P}^J_{M0}|\Phi(\beta_2)\rangle, \tag{8}$$

with a normalization factor f^J and projection operator $\hat{P}^J_{M0}$ written in terms of an integral over the Euler angles [42]. The energy E^J and f^J can be obtained by solving the Hill-Wheeler equation [42]. For axially symmetric nuclei the solution is simplified as [43]

$$E^J = \frac{\langle\Phi(\beta_2)|\hat{H}\hat{P}^J_{00}|\Phi(\beta_2)\rangle}{\langle\Phi(\beta_2)|\hat{P}^J_{00}|\Phi(\beta_2)\rangle}, \qquad f^J = \frac{1}{\sqrt{\langle\Phi(\beta_2)|\hat{P}^J_{00}|\Phi(\beta_2)\rangle}}. \tag{9}$$

The DRHBc theory provides a self-consistent description of deformed halo nucleus in the intrinsic frame without *a priori* decomposition of the core and halo, which are determined by analyzing the structure of SPLs after getting the ground state wave functions [15, 44]. According to the shapes of the core and halo density distributions, shape decoupling effects of deformed halos have been predicted in the MF level [15]. To examine how the core and halo behave in rotational states, one can calculate the one-body density of an excited state in coordinate space [45]

$$\rho^J(\boldsymbol{r}) = \left\langle \Psi^J \left| \sum_i \delta(\boldsymbol{r} - \boldsymbol{r}_i) \right| \Psi^J \right\rangle, \tag{10}$$

where the index i represents all occupied single particle sates of neutrons and protons.

Deformed halos and shape decoupling effects are attributed to the intrinsic structure of valence levels [15]. The configuration of the valence nucleon(s) is obtained by calculating the probability amplitude of spherical components of valence levels in the DRHBc+AMP approach. The Dirac WS basis [39] consists of spherical basis states labelled by $|nlj\rangle$ with the radial quantum number n, the orbital angular momentum l of the large component of the Dirac spinor, and the total angular momentum j. For each excited state, the probability amplitude of $|nlj\rangle$ is calculated as [46]

$$N^J_{nlj} = \frac{\langle \Phi(\beta_2)|\hat{N}_{nlj}\hat{P}^J_{00}|\Phi(\beta_2)\rangle}{\langle \Phi(\beta_2)|\hat{P}^J_{00}|\Phi(\beta_2)\rangle}, \tag{11}$$

where $\hat{N}_{nlj} = \sum_m c^\dagger_{nljm} c_{njlm}$ with m being the projection of total angular momentum on the symmetry axis.

3 Results and Discussions

In DRHBc calculations with the density functional PC-PK1, neutron-rich Mg isotopes ^{40}Mg, ^{42}Mg, and ^{44}Mg are well deformed with $\beta_2 = 0.46$, 0.38, and 0.31, respectively. The shell closure at $N = 28$ in Mg isotopes is quenched due to deformation effects. Figure 1 shows the single-particle levels (SPLs) of ^{42}Mg in the ground state and near the neutron Fermi energy λ_n. Valence neutrons partially occupy $\frac{1}{2}^-$ and $\frac{3}{2}^-$ levels, which are weakly bound or in continuum and contain considerable p-wave components, leading to the formation of halo. According to the structure of SPLs, the total density can be divided into the halo part contributed from weakly bound valence nucleons and the core part from the other tightly bound nucleons. In the first row of Figure 2, we show the densities of the whole nucleus, all neutrons, neutron core, and neutron halo in the xz plane from left to right for ^{42}Mg. One can see that the core has a prolate shape while the halo is slightly oblate, meaning that ^{42}Mg is a deformed halo nucleus with

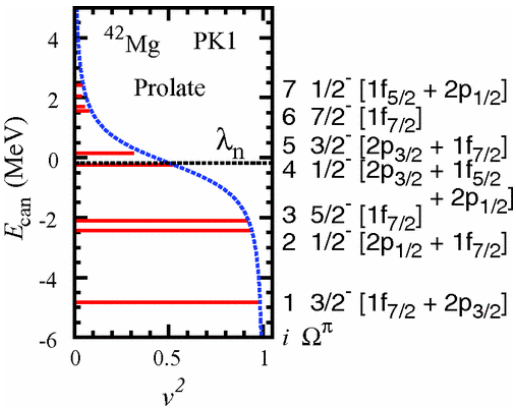

Figure 1. Single neutron levels with the quantum numbers Ω^π around the chemical potential (dotted line) in the canonical basis for ^{42}Mg as a function of the occupation probability. The order i, Ω^π, and the main WS components for orbitals close to the threshold are also given. The blue dashed line corresponds to the BCS-formula with an average pairing gap. Taken from Ref. [16].

shape decoupling effects. Similar results can be obtained for ^{44}Mg. More details about the halo structure of ^{42,44}Mg can be found in Refs. [15, 16].

After getting the mean-field ground state wave function, the excitation spectra can be calculated by using AMP. In DRHBc+AMP calculations, the excita-

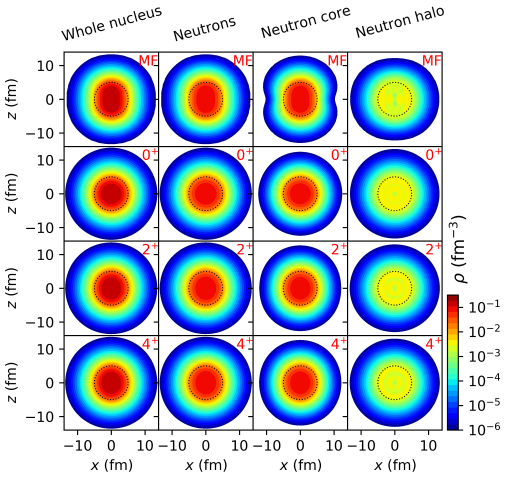

Figure 2. Densities for the whole nucleus, all neutrons, the neutron core, and neutron halo of ^{42}Mg in the MF ground state and projected 0^+, 2^+, and 4^+ states (with $M = 0$). Black dotted circles are given to guide the eye. Taken from Ref. [41].

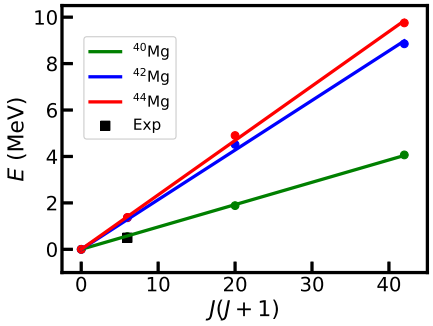

Figure 3. Excitation energies of collective states as a function of $J(J+1)$ for ^{40,42,44}Mg. The calculated results are labelled by solid dots and the linear fitting of calculated spectrum of each nucleus is shown by solid lines. The experimental result of ^{40}Mg taken from Ref. [47] is shown for comparison. Taken from Ref. [41].

tion energy of the 2^+ state of ^{40}Mg is 0.54 MeV, which is well consistent with the experimental value [47]. For halo nuclei ^{42}Mg and ^{44}Mg, there are no experimental spectra to date and the calculated values of $E(2^+)$ are all close to 1.40 MeV and much higher than that of ^{40}Mg. A typical feature of a rotational band is that the excitation energies hold a linear relation with $J(J+1)$, *i.e.*, $E(J^+) = \langle \hat{J}^2 \rangle / 2\mathcal{J}$ where $\mathcal{J}$ is the moment of inertia. We make a fit of the calculated excitation energies to this linear relation. The calculated excitation energies of ^{40,42,44}Mg and fitted lines are displayed in Figure 3. The distinct linear relation indicates that these three nuclei are all good rotors.

Taking ^{42}Mg as an example to show how the deformed halo evolves in rotational excitation, by using Eq. (10) the densities of projected states for the whole nucleus, all neutrons, the core, and halo are calculated and presented from the second row to the fourth row of Figure 2 for the 0^+, 2^+, and 4^+ states, respectively. We found that the neutron halo still exists in rotational excited states. All of these densities in the 0^+ state are spherical, meaning that there are no shape decoupling effects as a consequence of the nature of spherical symmetry of this state. In the 2^+ and 4^+ states, the core has prolate shapes while the halo is slightly oblate, indicating the appearance of shape decoupling effects in the 2^+ and 4^+ states.

The halo structure and shape decoupling effects are determined by intrinsic properties of valence levels [15–17]. To understand the halo configuration and behavior of shape decoupling effects in collective states, we take ^{42}Mg as an example again and calculate probability amplitudes of main spherical components in the neutron core and halo according to Eq. (11). The results are displayed in Figure 4. The valence neutrons are still dominated by p-wave with a considerable amplitude, resulting in the halo structure in collective states. Probability amplitudes of $2p_{1/2}$ and $1f_{5/2}$ in collective states almost keep unchanged compared with those of the MF ground state, while the amplitudes for $2p_{3/2}$ and

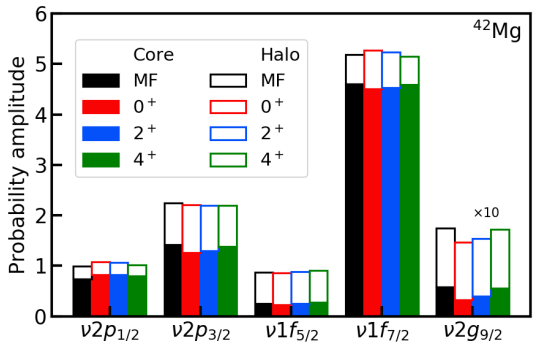

Figure 4. Probability amplitudes of p-, f-, and g-wave components contributed to the halo and core of the MF ground state and each collective state for ^{42}Mg. The probability amplitude of $\nu 2g_{9/2}$ is multiplied by 10. Taken from Ref. [41].

$1f_{7/2}$ decrease slightly with the increase of J. The probability amplitudes of p-, f-, and g-waves contributed to the neutron core also change slightly from the MF ground state to collective states. As a conclusion, the configuration of each low-lying rotational state of deformed halo nucleus is almost the same as that of the MF ground state, *i.e.*, the intrinsic structure of SPLs remains stable from the ground state in the intrinsic frame to the low-lying rotational states. Therefore, the halo natures persist from the ground state in the intrinsic frame to collective states and shape decoupling effects appear in 2^+ and 4^+ states. As for ^{44}Mg with a $4n$ halo, similar conclusions on the halo structure and shape decoupling effects can be obtained.

4 Conclusion

Based on the DRHBc theory which has been widely used to study ground state properties of deformed halo nuclei, the AMP technique has been implemented aiming at a self-consistent description of the rotational excitation of deformed halo nuclei. Deformed halos in Mg isotopes ^{42,44}Mg and their rotational properties are studied. By examining the density distributions and configurations of the intrinsic ground state and projected states, we found that the configuration of valence neutrons changes slightly from the MF ground state to collective states such that the halo structure persists from the ground state in the intrinsic frame to rotational states. As for shape decoupling effects of deformed halos, our study demonstrates that this exotic structure does not appear in the 0^+ state but exists in the 2^+ and 4^+ states. In future, other BMF corrections such as GCM and particle number projection can be considered for a better description for the excitation mode of deformed halo nuclei.

Acknowledgements

This work is supported by National Natural Science Foundation of China under Grants Nos. 12070131001, 12047503, 11961141004, 12175151, 12375118, and 12205308; China Postdoctoral Science Foundation (Grant No. 2022M713106); CAS Strategic Priority Research Program (XDB34010000); the IAEA Coordinated Research Project (F41033). The results described in this paper are obtained on the High-performance Computing Cluster of ITP-CAS and the ScGrid of the Supercomputing Center, Computer Network Information Center of Chinese Academy of Sciences.

References

[1] A.S. Jensen, K. Riisager, D.V. Fedorov, *et al.*, *Rev. Mod. Phys.* **76** (2004) 215-261.
[2] O. Sorlin, M.-G. Porquet, *Prog. Part. Nucl. Phys.* **61** (2008) 602.
[3] T. Frederico, A. Delfino, L. Tomio, *et al.*, Prog. Part. Nucl. Phys. **67** (2012) 939.
[4] I. Tanihata, H. Savajols, and R. Kanungo, *Prog. Part. Nucl. Phys.* **68** (2013) 215-313.
[5] S.-G. Zhou, *PoS* **INPC2016** (2017) 373.
[6] M. Freer, H. Horiuchi, Y. Kanada-En'yo, *et al.*, *Rev. Mod. Phys.* **90** (2018) 035004.
[7] T. Otsuka, A. Gade, O. Sorlin, *et al.*, *Rev. Mod. Phys.* **92** (2020) 015002.
[8] I. Tanihata, H. Hamagaki, O. Hashimoto, *et al.*, *Phys. Rev. Lett.* **55** (1985) 2676-2679.
[9] T. Nakamura, N. Kobayashi, Y. Kondo, *et al.*, *Phys. Rev. Lett.* **112** (2014) 142501.
[10] N. Kobayashi, T. Nakamura, Y. Kondo, *et al.*, *Phys. Rev. Lett.* **112** (2014) 242501.
[11] Z.H. Yang, Y. Kubota, A. Corsi, *et al.*, *Phys. Rev. Lett.* **126** (2021) 085501.
[12] K.J. Cook, T. Nakamura, Y. Kondo, *et al.*, *Phys. Rev. Lett.* **124** (2020) 212503.
[13] S. Bagchi, R. Kanungo, Y.K. Tanaka, *et al.*, *Phys. Rev. Lett.* **124** (2020) 222504.
[14] J. Meng, P. Ring, *Phys. Rev. Lett.* **77** (1996) 3963-3966.
[15] S.-G. Zhou, J. Meng, P. Ring, *et al.*, *Phys. Rev. C* **82** (2010) 011301(R).
[16] L.-L. Li, J. Meng, P. Ring, *et al.*, *Phys. Rev. C* **85** (2012) 024312.
[17] X.-X. Sun, J. Zhao, S.-G. Zhou, *Phys. Lett. B* **785** (2018) 530.
[18] X.-X. Sun, J. Zhao, S.-G. Zhou, *Nucl. Phys. A* **1003** (2020) 122011.
[19] X.-X. Sun, *Phys. Rev. C* **103** (2021) 054315.
[20] K. Zhang, M.-K. Cheoun, Y. B. Choi, *et al.*, (DRHBc Mass Table Collaboration) *Phys. Rev. C* **102** (2020) 024314.
[21] K. Zhang, M.-K. Cheoun, Y.B. Choi, *et al.*, (DRHBc Mass Table Collaboration) *At. Data Nucl. Data Tables* **144** (2022) 101488.
[22] C. Pan, M.-K. Cheoun, Y.B. Choi, *et al.*, (DRHBc Mass Table Collaboration) *Phys. Rev. C* **106** (2022) 014316.
[23] E. In, P. Papakonstantinou, Y. Kim, *et al.*, *Int. J. Mod. Phys. E* **30** (2021) 2150009.
[24] C. Pan, K. Zhang, S. Zhang, *Int. J. Mod. Phys. E* **28** (2019) 1950082.
[25] K. Zhang, X. He, J. Meng, *et al.*, *Phys. Rev. C* **104** (2021) L021301.
[26] C. Pan, K. Zhang, P.S. Chong, *et al.*, *Phys. Rev. C* **104** (2021) 024331.
[27] X.-T. He, C. Wang, K. Zhang, *et al.*, *Chin. Phys. C* **45** (2021) 101001.

[28] Y.B. Choi, C.H. Lee, M.-H. Mun, *et al.*, *Phys. Rev. C* **105** (2022) 024306.
[29] S. Kim, M.-H. Mun, M.-K. Cheoun *et al.*, *Phys. Rev. C* **105** (2022) 034340.
[30] P. Guo, C. Pan, Y.C. Zhao, *et al.*, *Phys. Rev. C* **108** (2023) 014319.
[31] K. Zhang, P. Papakonstantinou, M.-H. Mun, *et al.*, *Phys. Rev. C* **107** (2023) L041303.
[32] K. Zhang, S.Q. Yang, J.L. An, *et al.*, *Phys. Lett. B* **844** (2023) 138112.
[33] J.C. Pei, Y.N. Zhang, F.R. Xu, *Phys. Rev. C* **87** (2013) 051302(R).
[34] H. Nakada, K. Takayama, *Phys. Rev. C* **98** (2018) 011301(R).
[35] M. Bender, P.-H. Heenen, P.-G. Reinhard, *Rev. Mod. Phys.* **75** (2003) 121.
[36] T. Nikšić, D. Vretenar, P. Ring, *Prog. Part. Nucl. Phys.* **66** (2011) 519.
[37] J.M. Yao, J. Meng, P. Ring, *et al.*, *Phys. Rev. C* **79** (2009) 044312.
[38] K. Wang, B. Lu, *Commun. Theor. Phys.* **74** (2022) 015303.
[39] S.-G. Zhou, J. Meng, P. Ring, *Phys. Rev. C* **68** (2003) 034323.
[40] X.-X. Sun, S.-G. Zhou *Phys. Rev. C* **104** (2021) 064319.
[41] X.-X. Sun, S.-G. Zhou *Sci. Bull.* **66** (2021) 2072.
[42] P. Ring, P. Schuk, *The Nuclear Many-Body Problem*, Springer, Berlin (1980).
[43] M. Bender, P. Bonche, T. Duguet, *et al.*, *Phys. Rev. C*, **69** (2004) 064303.
[44] J. Meng, S.-G. Zhou, *J. Phys. G: Nucl. Part. Phys.* **42** (2015) 093101.
[45] J.M. Yao, M. Bender, P.-H. Heenen *Phys. Rev. C*, **91** (2015) 024301.
[46] Tomás R. Rodríguez, A. Poves, F. Nowacki, *Phys. Rev. C* **93** (2016) 054316.
[47] H.L. Crawford, P. Fallon, A.O. Macchiavelli, *et al.*, *Phys. Rev. Lett.* **122** (2020) 052501.